J Supercond Nov Magn (2017) 30:1161–1169
DOI 10.1007/s10948-016-3877-4

ORIGINAL PAPER

The Effect of *Ar* Ambient Pressure and Annealing Duration on the Microstructure, Superconducting Properties and Activation Energies of MgB_2 Superconductors

O. Ozturk[1,2] · E. Asikuzun[3] · S. Kaya[1] · N. S. Koc[4] · M. Erdem[4]

Received: 1 July 2016 / Accepted: 27 October 2016 / Published online: 19 December 2016

Abstract MgB_2 samples are produced by ex situ reaction method under vacuum, and various (0, 10, 20 Bar) Ar pressure for 0.5 and 1 h. The effect of ambient pressure and annealing duration on the microstructure and electrical properties of bulk samples are investigated. XRD, SEM, and magnetoresistance measurements are made. The *a* and *c* lattice parameters and the grain size values are the highest for the samples produced under vacuum and their values decrease with increasing Ar pressure. Moreover, these values increase when the annealing duration increases from 0.5 to 1 h. The increasing pressure reduces the bond lengths between the atoms thus the grain sizes decrease. Smaller grain size promotes the connection between grains which results in an increase of the critical current density (J_c). SEM micrographs reveal that the produced samples have granular structure which is a characteristic feature of MgB_2. The decrease of grain sizes and thus enhancement in grain connectivity with increasing pressure is also confirmed by SEM images. Magneto resistivity measurements show that T_c values of the samples produced under vacuum are the highest. T_c values decrease with increasing ambient pressure and applied magnetic field. The activation energies (U_0) of the samples are calculated using Arrhenius plots due to thermally activated flux flow theory. Existence and increase of Ar pressure causes increase of activation energies. The samples produced with 0.5-h annealing have higher activation energies than the ones produced with 1-h annealing.

Keywords Superconductivity · MgB_2 · Activation energy · Magnetoresistivity

1 Introduction

MgB_2 compound was discovered and synthesized in CALTECH in 1954 with XRD measurements [1]. The superconducting property of MgB_2 ($T_c = 39$ K) was announced by Jun Akimitsu [2]. Like other high-temperature superconductors, MgB_2 has layered structure and thus it is expected to have anisotropic properties. In its crystal structure, alternating layers of Mg and B atoms are aligned along the *c*-axis. It has AlB_2-type simple hexagonal structure in the P6/mmm space group [3].

It has a transition temperature T_c of 39 K which is lower than that of high-temperature superconductors, but it has the highest T_c among intermetallic compounds. The reason of high T_c is thought to be due to the vibrational frequency of the light B atoms. This proves that there are strong electron-phonon interactions in MgB_2. For industrial applications, the T_c should be higher and more importantly the current carrying capacity should be increased. Chemical additions intended to achieve these goals resulted in lowering of T_c and even destruction of superconductivity for higher amounts of additions [4–6]. Structural, mechanical,

✉ E. Asikuzun
easikuzun@kastamonu.edu.tr

1 Research and Application Center, Kastamonu University, 37100 Kastamonu, Turkey

2 Department of Physics, Kastamonu University, 37100 Kastamonu, Turkey

3 Department of Materials Science and Nanotechnology Engineering, Kastamonu University, 37100 Kastamonu, Turkey

4 Department of Physics, Abant Izzet Baysal University, 14280 Bolu, Turkey

and magnetic properties of the MgB_2 have been investigated in our previous studies [7, 8].

2 Experimental Details

In this study, commercial MgB_2 powder (Alfa Aesar, −325 mesh <44 micron) is used. Powder of 0.6 gr are pressed into pellets with 13-mm diameter and 1.0–1.5-mm thickness under 5 t of pressure. The obtained pellets are wrapped up tightly with Tantalium (Ta) folio. This was done to prevent oxidation and contamination of the samples. Then, they are put into a steel tube and after pumping of the air inside to obtain vacuum, they are heated to 850 °C with 5 °C/min ramping rate. Two sets of samples with 0.5 and 1 h of annealing times are obtained (*MgB-05-V* ve *MgB-1-V)*. Later, Ar flow is introduced into the tube and samples without ambient pressure are obtained at again 850 °C for 0.5 and 1 h of annealing times (*MgB-05-0B* and *MgB-1-0B*). For the final production stage, the tube is pressurized 10- and 20-bar Ar ambient pressure (*MgB-05-10B*,*MgB-05-20B*,*MgB-1-10B*, and *MgB-1-20B*). At the end of heating processes, the furnace is cooled from 850 °C down to the room temperature with a cooling rate of 5 °C/min. The produced samples are named as *MgB-05-V*,*MgB-05-0B*,*MgB-05-10B*,*MgB-05-20B*,*MgB-1-V*,*MgB-1-0B*,*MgB-1-10B*, and*MgB-1-20B*.

XRD measurements are made with Bruker D8 Advance model using CuKα ($\lambda = 1.5405$ Å) radiation to determine the crystal structure, main phase, and impurities in the samples. All the measurements are made in room temperature in the range $2\theta = 3$–$90°$ and with a scan speed of 0.6° /min XRD Evolution program is used to index the peaks and to calculate crystal parameters. The surface morphologies and the grain sizes are evaluated with JEOL 6390-LV SEM.

The electrical properties of the samples are determined by resistivity measurements under applied magnetic fields. Four point contacts are made by silver paste. The measurement are made in the temperature range 10–50 K and applied magnetic field range 0–5 T (0, 0.5, 1, 2, 3, 4, 5 T). The magnetic field is applied parallel to the 5-mA test current.

3 Results and Discussion

3.1 XRD Analyses

The XRD graphs of the samples are given in Fig. 1. From the figure, it can be clearly seen that all peak patterns belong to the main MgB_2 phase. The peaks are nearly at the same angles for all samples and no impurity phases are detected. For both series of samples, the peak intensities of

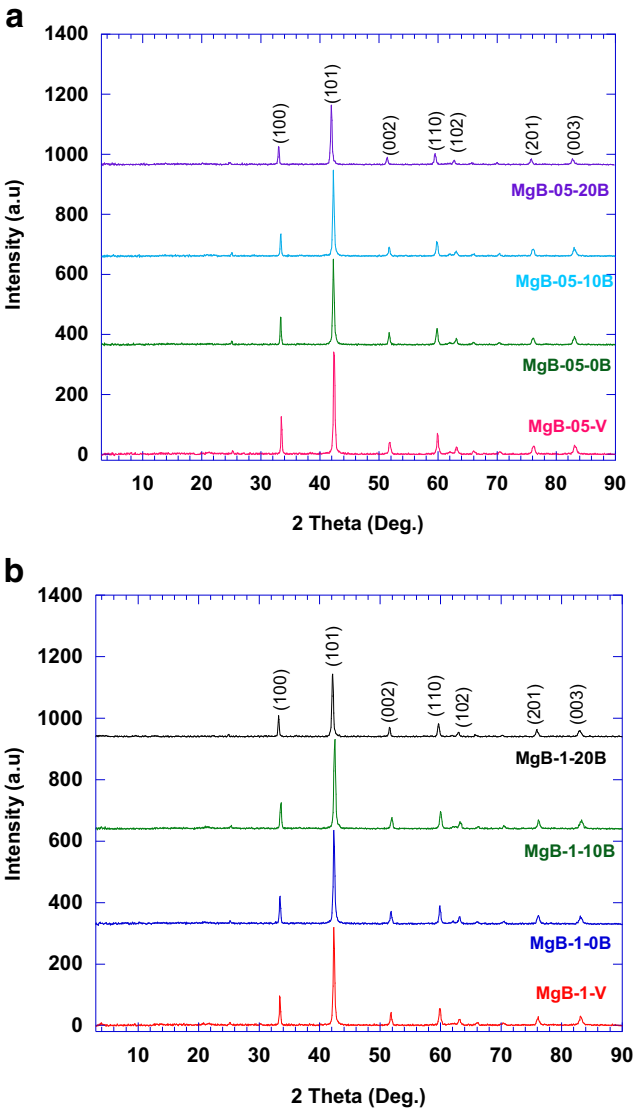

Fig. 1 XRD patterns of the samples

the vacuum-produced samples are higher and the peaks are narrower than those of the samples produced under ambient pressure. Increasing Ar pressure causes peak intensities to decrease and to increase the peaks wide. Better crystallinity of samples is observed under vacuum. The decrease in peak intensities may be due to the decrease in grain sizes as an effect of pressure. Using the XRD peaks of Fig. 1, a and c lattice parameters can be calculated via:

$$\frac{1}{d^2} = \frac{4\left(\square^2 + \square k + k^2\right)}{3a^2} + \frac{l^2}{c^2} \tag{1}$$

The results are tabulated in Table 1. Table 1 shows that both a and $c$lattice parameters decrease with Ar pressure increase. In previous studies, the applied pressure is confirmed to decrease the lattice parameters by shortening the

Table 1 *a* and *c* parameters, grain size values of all samples

Samples	*a* (Å)	*c* (Å)	Grain size (nm)
MgB-05-V	3.098	3.527	36.86
MgB-05-0B	3.096	3.511	35.76
MgB-05-10B	3.096	3.509	34.27
MgB-05-20B	3.092	3.506	31.57
MgB-1-V	3.099	3.537	38.94
MgB-1-0B	3.098	3.531	36.05
MgB-1-10B	3.097	3.520	35.15
MgB-1-20B	3.093	3.508	32.14

bond lengths [9–11]. Moreover, the change in the *c* lattice parameter is more than that of the *a* lattice parameter. This anisotropic behavior is due to the difference in the bond strengths along *a*and *c* directions in MgB_2. The covalent $B--B$ bonds along *a* direction are stronger than the *Mg–B* ionic bonds along the *c* direction [12].

Moreover, the samples annealed for 1 h have longer *a* and *c* parameters when compared to the ones annealed for 0.5 h. This can be explained with the increasing thermal expansion due to increased heat treatment time. Like other properties of MgB_2, anisotropy is seen in the change of lattice parameters. The change in *c* parameter is higher than the one in *a* parameter when the annealing time is increased which is consistent with previous studies [9].

The average grain sizes of the samples can be calculated using Scherer−Warren formula

$$D = 0941\lambda / B\cos\theta \tag{2}$$

$$B^2 = B_s^2 - B_m^2 \tag{3}$$

where *D* is the average grain size, λ is the wave length of the x-ray, $B_s$is the full width at half maximum (FWHM) in radians, B_m is a constant, and θ is the peak angle. The calculated values of grain sizes are given in Table 1. From the table, it is seen that the *MgB-05-V* and *MgB-1-V* samples have maximum values of grain sizes of 3686 and3894nm, respectively. The grain sizes decrease monotonously with the introduction of Ar and with the increase in pressure. The grain sizes decrease to 3157 and 3214nm for *MgB-05-20B* and *MgB-1-20B* samples, respectively, when the pressure reaches 20*B* Moreover, the grain sizes of *MgB-1* series are larger than the grain sizes of *MgB-05* series which means subjecting the samples for longer annealing time causes larger grain formation. This result is previously reported in the literature [13] and also confirmed by XRD and SEM results. As mentioned above, the pressure shortens the bonds between the atoms which results in grain size reduction. Smaller grain sizes are favorable for granular superconductors because small grains can have better grain connectivity which is essential for increasing critical current density (J_c) [14, 15].

3.2 SEM and EDS Analysis

The SEM images of the samples are given in Fig. 2. All samples have granular morphology peculiar to MgB_2. Variations of the grain sizes and aggregations can be seen from SEM images. Furthermore, we can observe that there is no particular orientation of the grains.

The grains of 1-h annealed samples are obviously larger than those of the 0.5-h annealed ones. The increase in annealing time and temperature causes larger grain formation [13]. As confirmed by grain size calculations, increasing Ar ambient pressure results in smaller grains. The voids decrease and connectivity between grains increase due to the reduction in grain sizes. Moreover, the porosity also decreases with decreasing grain sizes which directly affects the mechanical properties of the samples.

EDS measurements are also made in order to analyze the change in the ionic quantity of the samples with heat treatment and pressure. The results are given in Fig. 3 for the samples MgB-05-V, MgB-1-V, *MgB-05-10B*, and *MgB-1-10B*. Due to these results, Mg, B, and small amount of O elements are detected (Table 2). Although commercial powder was used in this study, the presence of oxygen indicates that small amount of impurity phases are present. As can be seen from the table, the amount of oxygen in 1-h annealed samples is higher than that of the 0.5-h annealed samples which indicates that the increase in annealing time increases oxygen content in the samples.

3.3 Magnetoresistivity Measurements

The resistivity ($\rho - T$) measurements under varying applied magnetic fields are made to investigate the magnetoresistivity behavior of the samples. All measurements are made in the 10–50 K temperature range and 0–5 Tesla magnetic field range. The results of the *MgB-05-V*,*MgB-05-20B*,*MgB-1-V*, and *MgB-1-20B* samples are given in Fig. 4. The T_c^{offset} values, where the resistivity drops to zero are determined from the $\rho - T$ graphs and the results are tabulated in Table 3. The samples have metallic behavior above the T_c^{onset} transition temperature. The transition temperature values change as a function of applied magnetic field. For all samples, theT_c^{onset} and T_c^{offset} values decrease with increasing applied magnetic field. The applied magnetic field penetrates into the superconductor at the grain boundaries where the grains are weakly connected. Thus, as the magnetic field is increased, the deteriorating effect of non-superconducting weak links increases. The resistivity results clearly shows that the samples produced in vacuum have the highest transition temperatures. The $T_c$values decrease with increasing Ar pressure. The 1-h annealed samples have lower T_c values than the 0.5-h annealed samples.

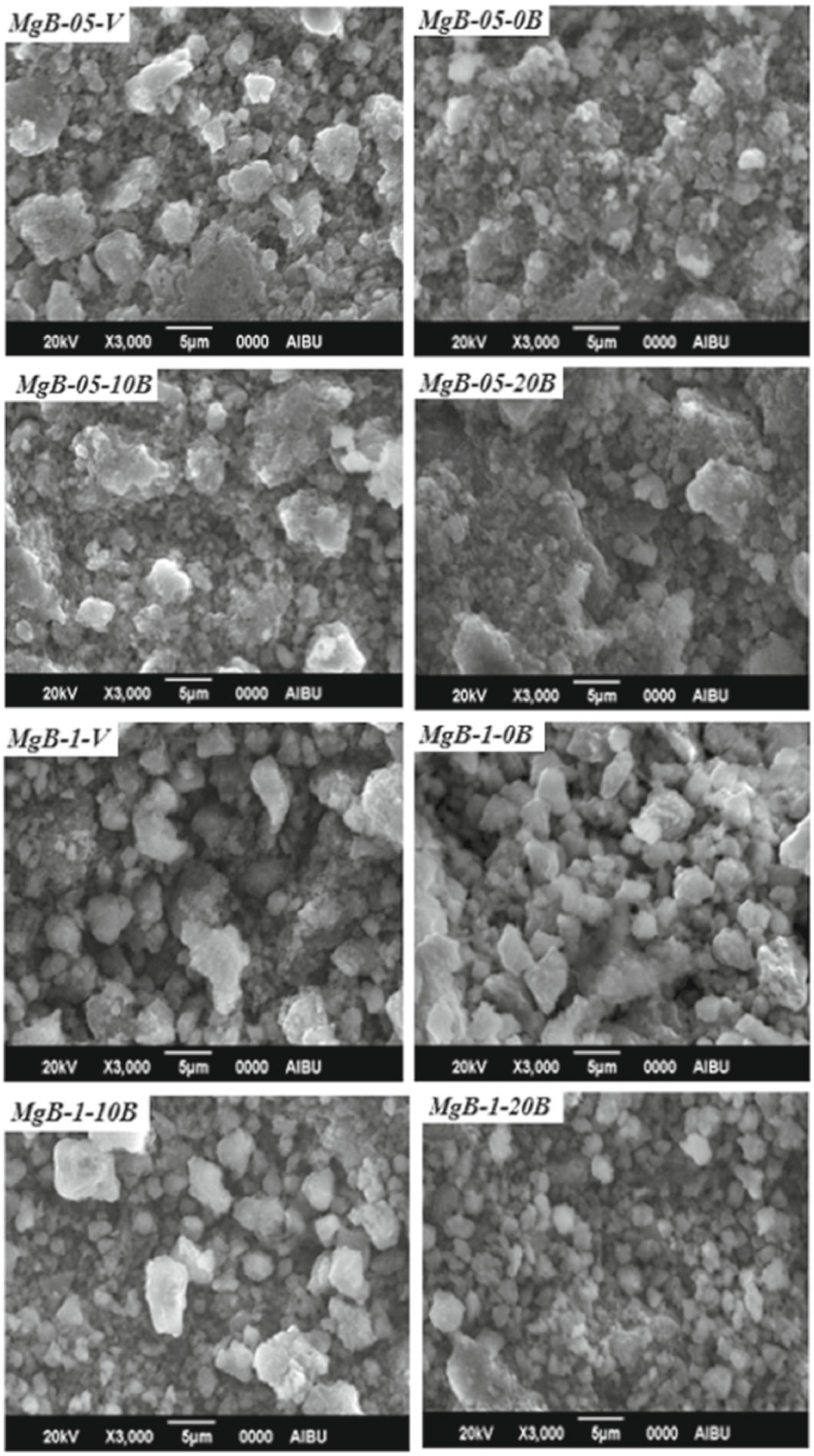

Fig. 2 SEM micrographs of the samples

The decrease of T_c values with increasing pressure is observed in many previous studies [16–19]. Similarly, the decrease of T_c with pressure in MgB_2 superconductor is reported in the literature [10, 20]. The decrease of T_c with pressure endorses the idea that there is BCS-type coupling originating from high phonon frequency of the B element in

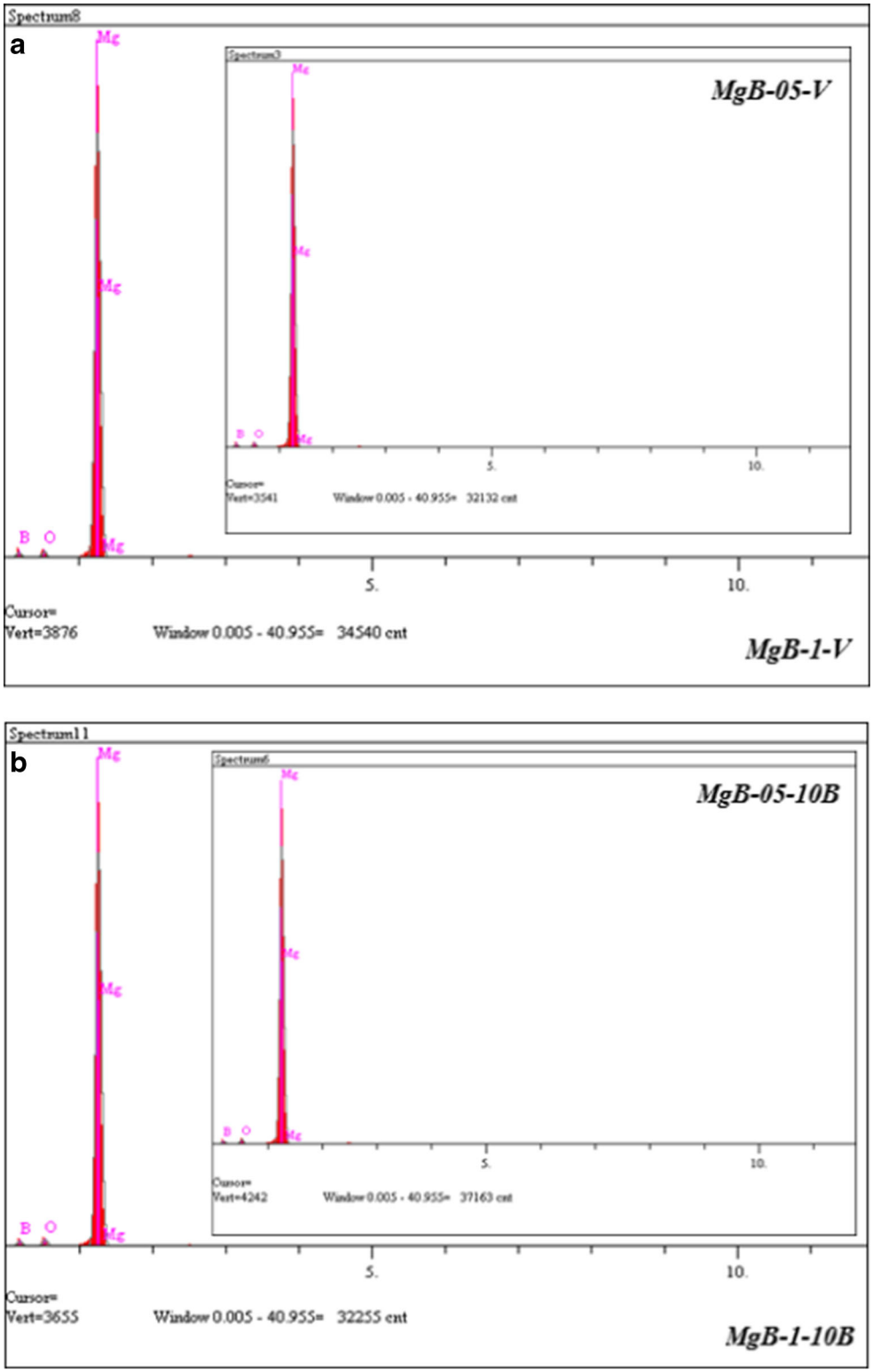

Fig. 3 EDS graphs of *MgB-05-V*, *MgB-1-V*, *MgB-05-10B* and *MgB-1-10B* samples

MgB_2 compound [21]. This result shows that the decrease in the density of states at the Fermi energy due to the contraction of the $B--B$ and B–Mg bonds is dominant over the increase in the phonon frequency which would raise the T_c.

Table 2 Results of *EDS* analysis of *MgB-05-V*, *MgB-1-V*, *MgB-05-10B* and *MgB-1-10B* samples

Samples	Elt.	Intensity (c/*s*)	Conc.
MgB-05-V	*B*	7.02	68.839
	O	9.13	4.422
	Mg	713.88	26.739
MgB-1-V	*B*	8.78	70.502
	O	10.08	4.364
	Mg	760.66	25.136
MgB-05-10B	*B*	7.00	67.19
	O	10.57	4.61
	Mg	821.17	28.19
MgB-1-10B	*B*	8.17	70.01
	O	10.89	5.00
	Mg	702.28	24.97

Table 3 T_c^{offset} values of the samples under the magnetic field

Samples	T_c^{offset} (K)						
	0 T	0.5 T	1 T	2 T	3 T	4 T	5 T
MgB-05-V	38.44	38.00	36.77	35.55	34.44	33.66	31.94
MgB-05-0B	38.41	37.87	36.50	35.22	34.32	33.08	31.90
MgB-05-10B	38.29	37.22	36.36	35.16	33.75	32.61	31.36
MgB-05-20B	37.93	37.44	35.22	34.80	33.33	32.43	31.32
MgB-1-V	39.74	38.30	37.48	36.13	35.75	34.88	32.06
MgB-1-0B	38.30	38.22	37.21	36.00	34.93	33.61	31.99
MgB-1-10B	38.04	36.66	35.83	34.33	33.61	32.63	30.33
MgB-1-20B	35.88	35.13	34.72	33.47	32.00	31.25	30.27

3.4 Activation Energy

The flux pinning property is essential in superconductors. The flux pinning ability can be calculated using flux pinning force density or activation energy [22, 23]. Activation energy (U_0) is the potential energy barrier preventing flux motion at the pinning centers. Activation energy can be calculated using *Arrhenius* equation of the thermally assisted flux (TAF) [24, 25].

$$\rho(BT) = \rho_0 \exp?(-U_0(B,T))/k_B T) \quad (4)$$

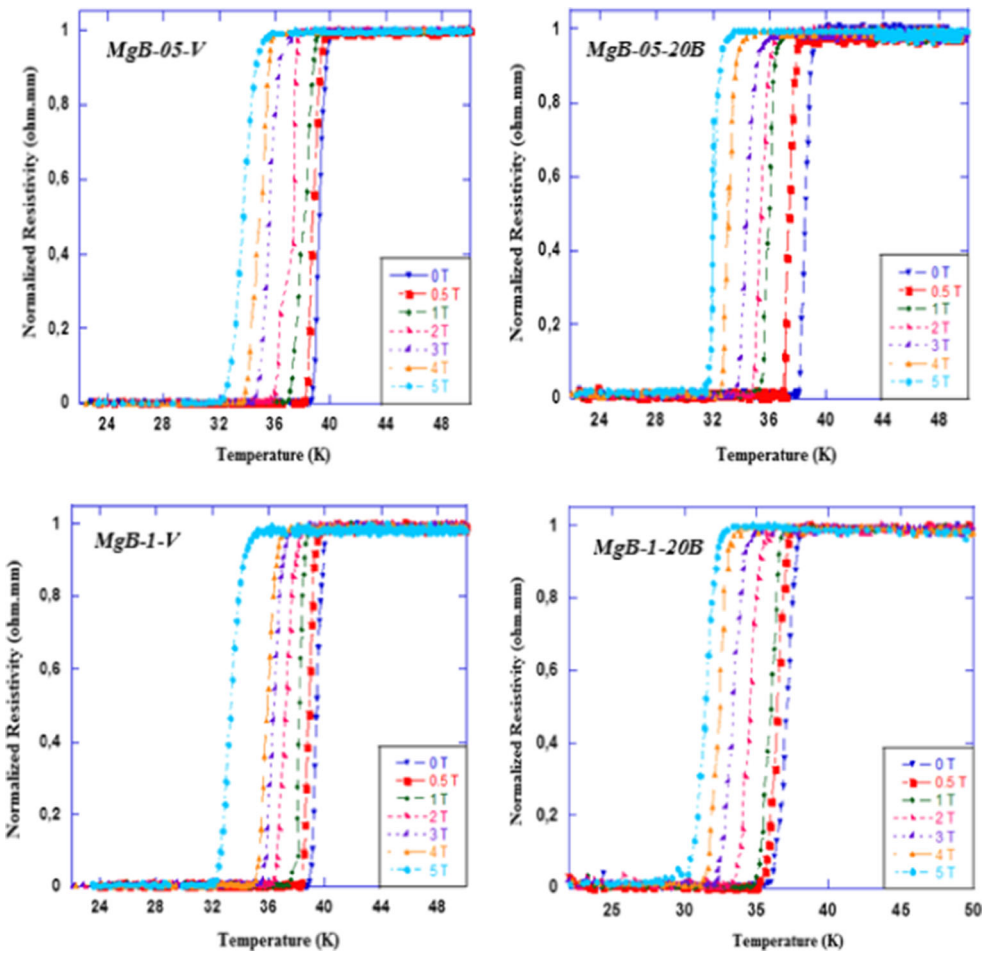

Fig. 4 Normalized resistivity as a function of temperature curves for the samples under different magnetic fields

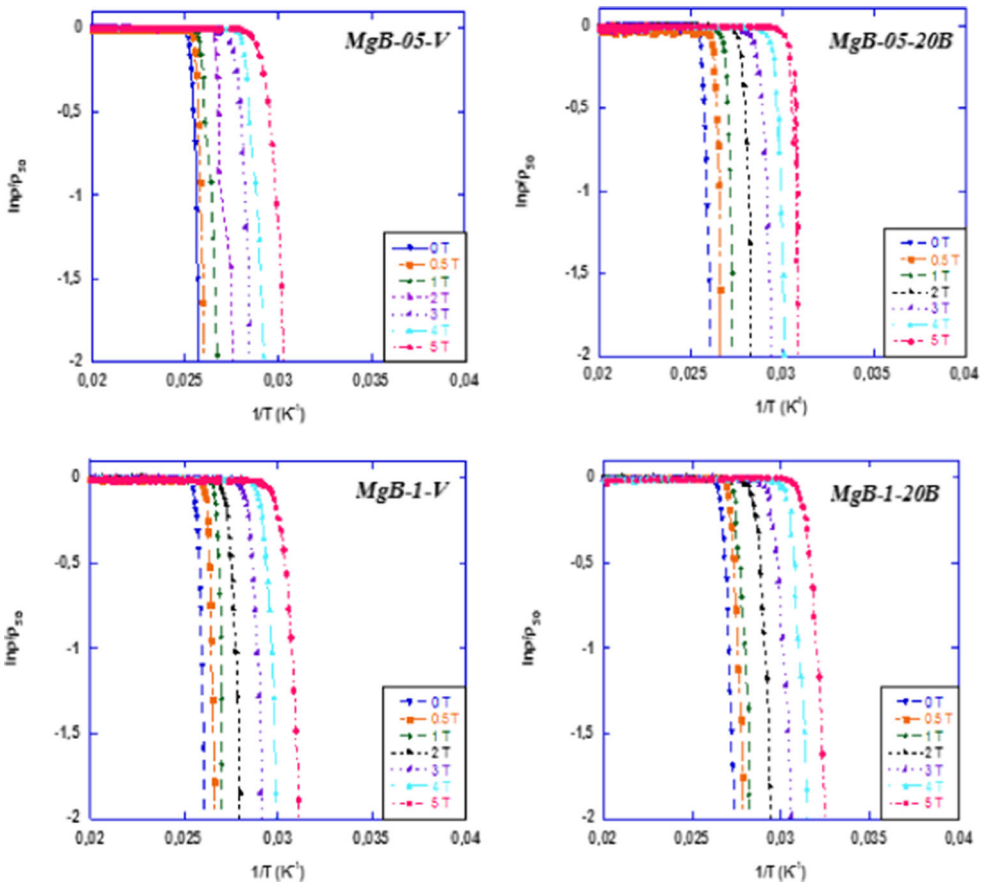

Fig. 5 Variation of *In* (ρ/ρ_0) vs. *1/T* (K^{-1}) for the *MgB-05-V*,*MgB-05-20B*,*MgB-1-V*, and *MgB-1-20B* samples

where ρ_0 is the field-independent exponential factor, $U_0$is the activation energy, and k_B is the Boltzman constant. The activation energy is a function of both applied magnetic field and temperature which can be written as$U_0\,(B,\,T) = U_0\,(B)\,U_0(T)$. The temperature dependence of the activation energy is given by the function $U_0\,(T) = \left(1 - T/T_p\right)^m$. The fitting of the In $\rho\,/\rho_0$ vs. $1\,/T$ graph is known as *Arrhenius plot* (Fig. 4). The slope of the linear part in the tail of this graph gives the magnetic field dependent activation energy $U_0(B)$ [26, 27]. The ln $\rho\,/\rho_0$ vs. $1\,/T$ graphs for all samples under varying applied magnetic fields (0–5 T) are given in Fig. 5, and the calculated activation energies are tabulated in Table 4.

The activation energies of the samples increase when Ar is introduced and with the increase of Ar pressure. The U_0 (0, T) values of vacuum produced *MgB-05-V* and *MgB-1-V* samples are 8769 and 7345 K, respectively. The activation energy values increase to 9902 and 9521 K for *MgB-05-20B* and *MgB-1-20B* samples, respectively. The increase in activation energies can be explained by the decrease in the grain sizes and voids due to the applied pressure. The applied pressure results in the increase of density of the samples, better interface microstructure and stronger grain connectivity. These results are also supported by SEM results. All these parameters are essential for obtaining high J_c values in the samples [28].

There are differences in the activation energies of the samples which are produced with different annealing times. Table 4 reveals that the series of samples produced with 0.5 h of annealing (*MgB-05*) have higher U_0values than the samples produced with 1 h of annealing (*MgB-1*). Longer annealing times causes increase in porosity, grain sizes, and

Table 4 Activation energies of the samples under the magnetic field

Samples	Activation energies (K)						
	0 T	0.5 T	1 T	2 T	3 T	4 T	5 T
MgB-05-V	8769	7472	6811	5438	4171	3215	2644
MgB-05-0B	9295	8657	8006	6437	5418	4280	3486
MgB-05-10B	9673	9232	8531	7316	6410	5249	4253
MgB-05-20B	9902	9507	8891	7478	6816	5444	3689
MgB-1-V	7345	6813	5943	4535	3934	2856	1778
MgB-1-0B	8690	7989	7076	6014	5142	4027	2956
MgB-1-10B	9102	8428	7549	6678	5594	4790	3810
MgB-1-20B	9521	8992	7989	6984	6042	5306	4215

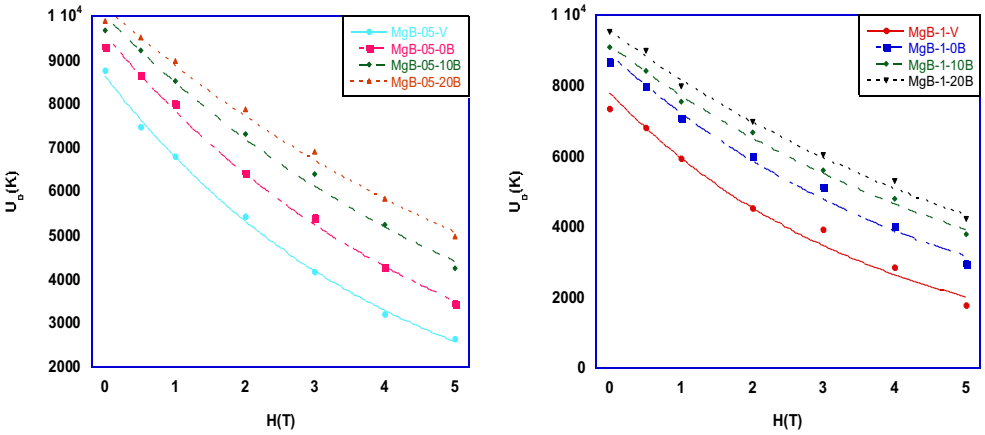

Fig. 6 Variation of $U_0\,(K)$ vs. $H(T)$ for all samples

the voids between grains which result in reduction in the pinning ability of the superconductors [26, 28, 29].

Moreover, the activation energies of the samples decrease with increasing applied magnetic field as shown in Fig. 6. This is an expected result because by increasing magnetic field, more flux lines penetrate into the superconductor which acts to deteriorate superconductivity [29].

4 Conclusion

MgB_2 superconducting samples are produced by ex situ method in vacuum, in *Ar* atmosphere at 0-, 10-, and 20-Bar pressures with 0.5- and 1-h annealing times. The effects of pressure and annealing time on the microstructure and electrical properties of the samples are analyzed by XRD, SEM, EDS, and magnetoresistivity measurements and the following results are obtained:

- XRD results show that transition from vacuum to *Ar* atmosphere and increasing pressure cause the *a* and *c*lattice parameters to decrease. Due to the difference in bond strengths along *a* and *c* directions, the change in *c* parameter is higher than that of the *a* parameter—a result associated with the anisotropy of the MgB_2.
- The grain sizes of the samples decrease with increasing pressure. The increase in annealing time causes an increase in the grain sizes. These results are confirmed both by XRD and SEM results.
- $\rho - T$ measurements under applied magnetic field show that T_c^{onset} and T_c^{offset} values decrease with increasing applied magnetic field. The samples produced in vacuum have higher T_c values than the ones produced in *Ar* ambient pressure.
- The activation energy values increase when samples are subjected to *Ar* atmosphere and with increasing *Ar* pressure.
- The activation energies of the 0.5-h annealed samples are higher than those of the 1-h annealed samples.
- Increasing the applied magnetic field reduces the activation energies as expected.

Acknowledgments This study is supported by Kastamonu University Scientific Research Fund (BAP) with project code KÜBAP-03/2012-03.

References

1. Jones, M.E., Marsh, R.E.: J. Am. Chem. Soc. **76**, 1434–1436 (1954)
2. Nagamatsu, J., Nakagawa, N., Muranaka, T., Zentiani, Y., Akimitsu, J.: Nature **410**, 63–64 (2001)
3. Buzea, C., Yamashita, T.: Supercond. Sci. and Technol. **14**, 115–146 (2001)
4. Kazakov, S.M., Puzniak, R., Rogacki, K., Mironov, A.V., Jun, J., Zhigadlo, N.D., Soltmann, C.H., Batlogg, B., Karpinski, J.: Phys. Rev. B **71**, 024533 (2005)
5. Slusky, J.S., Rogado, N., Regan, K.A., Hayward, M.A., Khalifah, P., He, T., Inumaru, K., Lourerio, S.M., Haas, M.K., Zandbergen, H.W., Cava, R.J.: Nature **410**, 343–345 (2001)
6. Mickelson, W., Cumings, J., Han, W.Q., Zettl, A.: Phys. Rev. B **65**, 052505 (2002)
7. Ozturk, O., Asikuzun, E., Kaya, S., Erdem, M., Safran, S., Kilic, A., Terzioglu, C.: J. Supercond. Nov. Magn. **28**, 1943–1952 (2015)
8. Ozturk, O., Asikuzun, E., Kaya, S.: J. Mater. Sci. Mater. Electron. **26**(6), 3840–3852 (2015)
9. Jorgensen, J.D., Hinks, D.G., Short, S.: Phys. Rev. B **63**, 224522 (2001)
10. Vogt, T., Schneider, G., Hriljac, J.A., Yang, G., Abell, J.S.: Phys. Rev. B **63**, 220505 (2001)
11. Zhang, C., Zhang, X.: Comput. Mater. Sci. **50**, 1097–1101 (2011)
12. Schneider, T., Di Castro, D.: Phys. Rev. B **72**, 054501 (2005)
13. Dogruer, M., Gorur, O., Zalaoglu, Y., Ozturk, O., Yildirim, G., Varilci, A., Terzioglu, C.: J. Mater. Sci. Mater. Electron. **24**, 352–361 (2012)
14. Larbalestier, D., Gurevich, A., Feldmann, D.M., Polyanskii, A.: Nature **414**, 368–377 (2001)
15. Kambara, M., Hari Babu, N., Sadki, E.S., Cooper, J.R., Minami, H., Cardwell, D.A., Campbell, A.M., Inove, I.H.: Superc. Sci. Tech. **14**, 5–7 (2001)

16. Gubser, D.U., Webb, A.W.: Phys. Rev. Lett. **35**, 104–107 (1975)
17. Jennings, L.D., Swenson, C.A.: Phys. Rev. **112**, 31–43 (1958)
18. Wittig, J.: Z. Phys. **195**, 27–215 (1966)
19. Il'ina, M.A., Itskevich, E.S. Zh. Eksp. Teor. Fiz **61**, 2357–2361 (1971)
20. Bordet, P., Mezouar, M., Nunez-Regueiro, M., Monteverde, M., Nunez-Regueiro, M.D., Rogado, N., Regan, K.A., Hayward, M.A., He, T., Loureiro, S.M., Cava, R.J.: Phys. Rev. B **64**, 2502 (2001)
21. Hirch, J.E., Marsiglio, F.: Phys. Rev. B **64**, 144523 (2001)
22. Pu, M.H., Song, W.H., Zhao, B., Wu, X.C., Sun, Y.P., Du, J.J., Fang, J.: Phys. C **361**, 181–188 (2001)
23. Vinu, S., Sarun, P.M., Shabna, R., Syamaprasad, U.: J. Alloys Compd. **487**, 1–4 (2009)
24. Anderson, P.W.: Phys. Rev. Lett. **9**, 309 (1962)
25. Anderson, P.W., Kim, Y.B.: Rev. Mod. Phys. **36**, 39 (1964)
26. Abou-Aly, A.I., Mahmoud, S.A., Awad, R., Barakat, M.M.E.: J. Supercond. Nov. Magn. **23**, 1575–1588 (2010)
27. Abou-Aly, A.I., Korayem, M.T., Gomaa, N.G., Awad, R., Al-Hajji, M.A.: Supercond. Sci. Technol. **12**, 147 (1999)
28. Vo, N.V., Liu, H.K., Dou, S.X.: Supercond. Sci. Technol. **9**, 104 (1996)
29. Abou-Aly, A.I., Awad, R., Mahmoud, S.A., Baraka, M.M.: J. Supercond. Nov. Magn. **25**, 451–461 (2012)